24th COBEM - 2017

24th ABCM International Congress of Mechanical Engineering
December 3-8, 2017, Curitiba, PR, Brazil

COBEM-2017-0823
HYDRODYNAMIC AND ACOUSTIC CHARACTERISTICS OF LABHIDRO'S SMALL CAVITATION TUNNEL

Walfrido Barnack Neto
Alceu José dos Santos Moura
Ricardo Sbragio
Hélio Corrêa da Silva Júnior
Leandro Pansanato

Hydrodynamic Laboratory, Diretoria de Desenvolvimento Nuclear da Marinha, Av. Prof. Lineu Prestes 2468, SP
barnack.neto@marinha.mil.br
alceu.moura@marinha.mil.br
sbragio@marinha.mil.br
helio.correa@marinha.mil.br
pansanato@marinha.mil.br

Abstract.*This work presents the general characteristics of the small cavitation tunnel (SCT) of the Hydrodynamic Laboratory (LABHIDRO) and the investigation of its hydrodynamic and acoustic performance. The design of the impeller is outlined. Both numerical simulations and experimental methods were applied for the assessment of the velocity in the test section. Investigation about head losses and acoustics of the flow and structure interaction are also presented.*

Keywords:*cavitation tunnel, impeller design, hydrodynamic noise, acoustics, hydrodynamics.*

1. INTRODUCTION

The Hydrodynamic Laboratory (LABHIDRO) is aimed to provide experimental support in hydrodynamics for the Brazilian Navy. Among its facilities, LABHIDRO operates a Small Cavitation Tunnel (SCT). In 2011, the SCT was upgraded by the installation of a new impeller. Figures 1, 2 and 3 present the schematics and pictures of the tunnel.

The SCT was conceived as a test tool for providing information for the construction of a larger cavitation tunnel. The main objective of SCT is the impeller project development and tests, regarding its hydrodynamic performance and acoustic characteristics. The SCT's other objectives include flow acoustic investigation, CFD evaluation, and operation training.

The upper part of the SCT is made of acrylic for flow visualization; the lower part is made of carbon steel. The test section in the upper part is 25 cm wide and 18 cm high. An acoustic chamber is located below the test section.

The impeller is driven by a brushless permanent magnet motor encapsulated within a sealed pod.

This article aims to present the SCT's characteristics, the design of the impeller and some acoustic and hydrodynamic characteristics obtained by experimental and computational methods.

Figure 1.Picture of the SCT at LABHIDRO.

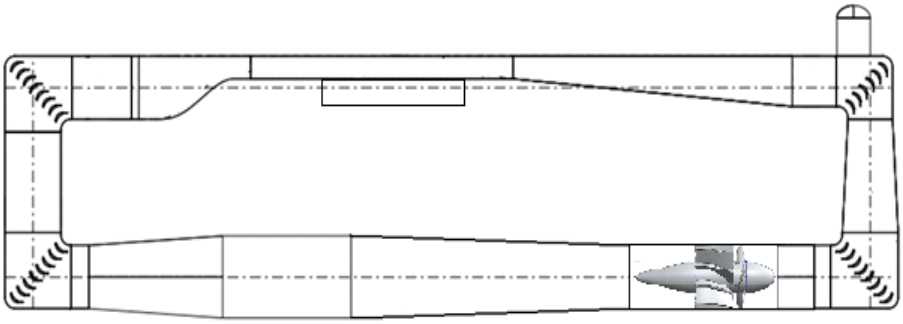

Figure 2. Schematics of the SCT with the impeller highlighted.

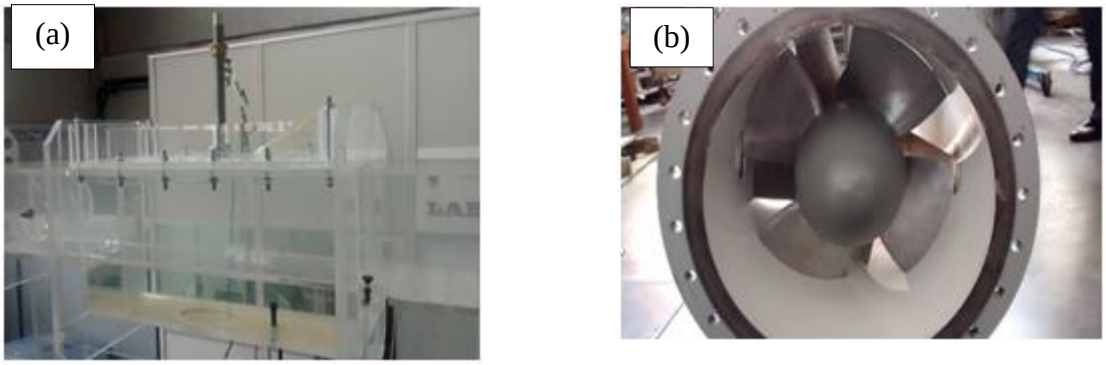

Figure 3.SCT details. (a) test section; (b) impeller.

2. RATIONAL DESIGN OF THE IMPELLER

The design parameters of the impeller are:

a) Test section mean velocity: 6 m/s;
b) Podded motor drive;
c) Low noise operation.

The circulation theory approach was applied for the hydrodynamic design of the impeller.

The flow head loss in the cavitation tunnel was estimated according to Idelchik(1986) and totalizes approximately 8000 Pa at 300rpm. The test section and diffuser share 77% of the total head losses.

The impeller was design with 4 blades, and a stator with 9 fixed blades, which supports the impeller inside the tunnel and reduces the flow rotation.

3. EXPERIMENTAL PROCEDURE

3.1 Acoustic measurements

These tests were focused in the noise generation by the impeller. Both the acoustic pressure generated outside the cavitation tunnel close to the impeller and the hydrodynamic noise in the acoustic chamber where acquired.

For the noise generated close to the impeller, a microphone was used while the hydrodynamic noise was registered by a hydrophone in the acoustic chamber, which is placed bellow the test section.

Both transducers aimed to quantify the sound pressure level of the noise produced by the impeller, in order to verify if the design cope with noise reduction requirements.

3.2 Velocity profile in the test section

The velocity profile in the test section was retrieved in order to obtain experimental data for comparison with CFD calculations. The velocity distribution was estimated by using the differential pressure measured by a movable Pitot tube along the test section with a mercury column manometer. Figure 4 presents the velocity measurement apparatus.

Figure 4. Velocity measurement apparatus: (a) Pitot tube in test section and the hydrophone at the acoustic chamber below; (b) Mercury column manometer.

The mean velocity in the center of the test section was measured by differential pressure with pitot tube and a mercury column manometer. The relation between the column of mercury and the differential pressure is shown in Eq. (1):

$$p_{columnHg} = \rho_{Hg} g h \tag{1}$$

Where $p_{columnHg}$ is the pressure measured at the mercury column manometer; ρ_{Hg} is the specific mass of Mercury; g is the acceleration of gravity; and h is the unbalance at the mercury column manometer.

The velocity in the center of test section is calculated by Eq. (2) and Eq. (3):

$$\frac{1}{2}\rho_{H2O} v^2 = p_{columnHg} \tag{2}$$

$$v = \sqrt{\frac{2p_{columnHg}}{\rho_{H2O}}} \tag{3}$$

Where ρ_{H2O} is the specific mass of fresh water; and v is the flow velocity.

3.3 Head loss

The head losses were estimated by the differences in the total pressure using Pitot tubes in the upstream and downstream flow at the impeller section as shown in Fig. 5. For the other parts of the tunnel the head losses were estimated according to Idelchik (1986). The rotation range varied from 50 to 300 rpm.

Figure 5.Impeller section with the pitot tubes highlighted in red circles.

4. CFD COMPUTATIONAL PROCEDURE

The internal flow in the test section was evaluated by CFD and compared with the measurements. The calibrated CFD model will be a design tool for the Large Cavitation Tunnel (LCT). The solver used is ANSYS FLUENT®.

4.1 Geometric characteristics

In the CFD analysis of the flow in the test section, in order to reduce the flow domain, only the contraction, test section and upper diffuser were modelled. Figure 6 highlights the selected domain.

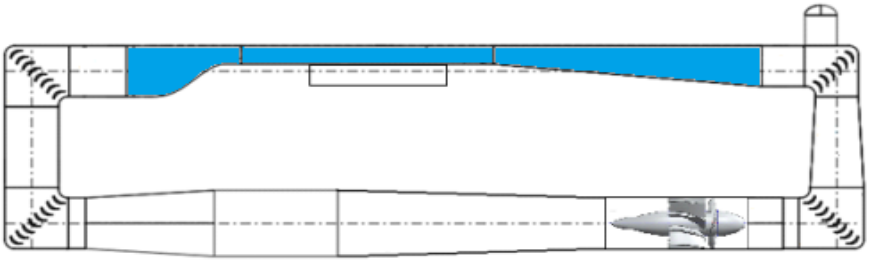

Figure 6. CFD Domain highlighted.

4.2 Grid overview

For this analysis, three different hexahedral grids were generated. An overview of the grid lay-out and cell distribution in the domain is presented in Fig. 7. In order to resolve the boundary layer, wall functions were used, and a first cell height was applied which results in a dimensionless wall distance (y+) of the order of 30 to 300 for all grids. The number of cells in the complete domain and also the y+ value is presented in Tab. 1.

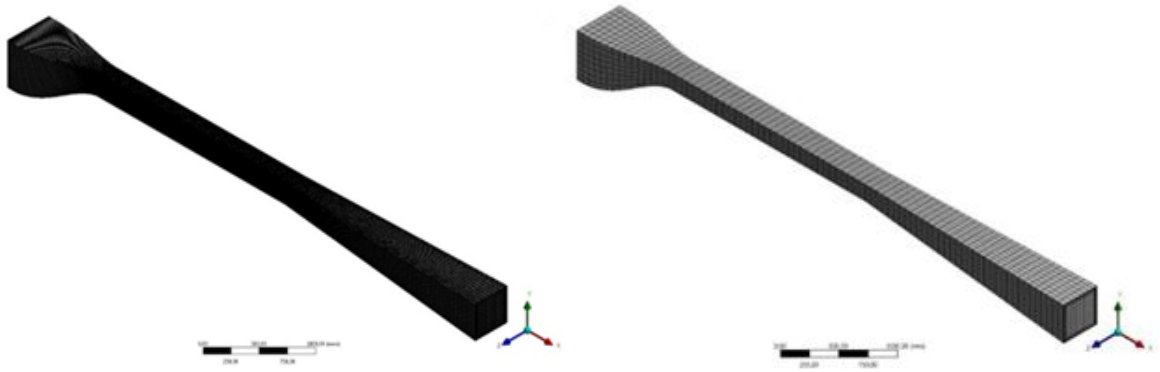

Figure 7.Overview of domain grid for refined mesh G3 (left) and for coarse mesh G1 (right).

Table 1.Overview of grid density and maximum y+ values.

Mesh Id	Number of interior cells	y+
G1	181.10^3	298
G2	781.10^3	175
G3	$3.156 .10^6$	32

4.3 Numerical set-up

At the inlet, a uniform velocity is specified with a low turbulence level. At the outlet an outflow boundary condition is specified with the gradient in normal direction set to zero for all flow variables. A no-slip condition is used in the walls.

The simulations were performed using the viscous CFD code Fluent 17.1. Relevant numerical settings used for the simulations are listed in Tab. 2.

Table 2. Overview of numerical settings used in the simulations.

General		
Density	997.2994	Kg/m^3
Dynamic Viscosity	9.1100e-4	Kg/(m.s)
Transport equations		
Mass momentum solver	Coupled	
Momentum discretization	Second Order Upwind	
Turbulence discretization	Second Order Upwind	
Turbulence model	k-ω SST	

5. RESULT ANALYSIS

5.1 Acoustic measurement results

The acoustics tests carried out in the SCT allowed the verification of the influence of the blade pass frequencies (BPFs) of the rotor/stator setup in the resonance peak at an specific rotation velocity of the impeller. In this case, the rotation velocity was 209 rpm. The resonance peak registered by the acoustic pressure transducer has a frequency of 251.2 Hz, corresponding to the second harmonic of the BPF in 209 rpm, as shown in Eq. 4. The microphone was not able to detect first harmonic component. However, the hydrophone captured both the first and the second harmonic. Figure 8 presents the peak response of the microphone at 251.2 Hz.

$$f = N_r N_s \, nN_{harm}/60 \tag{4}$$

Where f is the acoustic response frequency (Hz); N_r is the rotor number of blades (4 blades); N_s is the stator number of blades (9 blades); n is the impeller revolutions in rpm (209 rpm); and N_{harm} is the harmonic number (2nd harmonic).

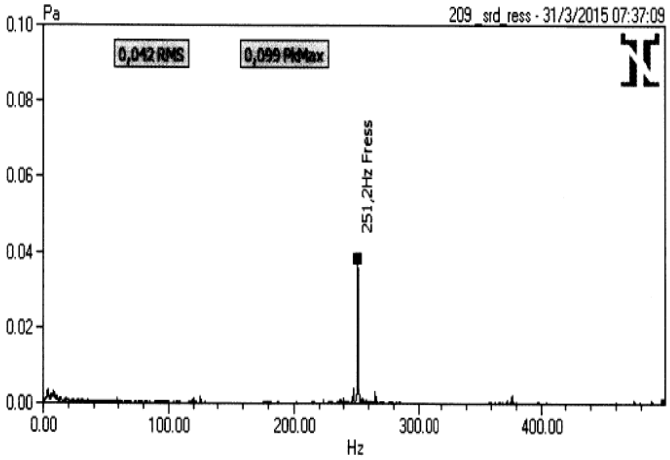

Figure 8.Peak response of acoustic pressure in the impeller in 209 rpm.

5.2 Velocity measurement results

The velocity in the test section was measured by the Pitot tube. The results for mean velocity as a function of the rotation of the impeller are presented in Fig. 9. The mean velocity behaves quite linearly with the impeller rotation.

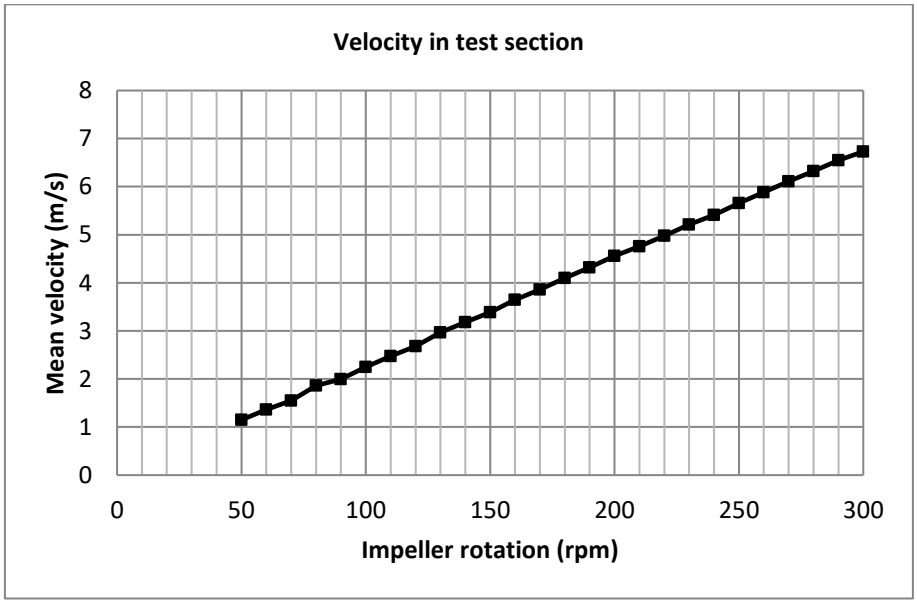

Figure 9. Mean velocity in test section.

The velocity profile in the test section for an impeller rotation of 200 rpm is shown in Fig. 10.

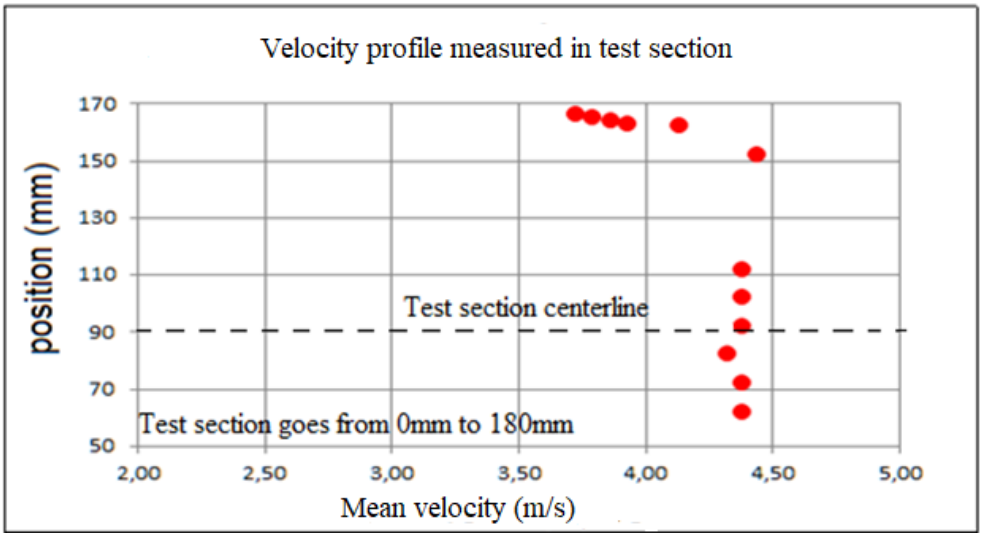

Figure 10.Measured Velocity profile in the test section for 200 rpm.

5.3 Head loss

The total head loss was estimated analytically, according to the methodology presented in Idelchik (1986) and compared with measurements of the partial head loss of all sections, except the impeller section, added with an analytic estimation of the head loss in the impeller section. This procedure was adopted because the arrangement of the pitot tubes does not allow the measurement in the impeller section. As the head loss of the impeller section is less than 5% of the total head loss, this procedure is considered adequate. Figure 11 presents the comparison of numerical estimation and the measurements.

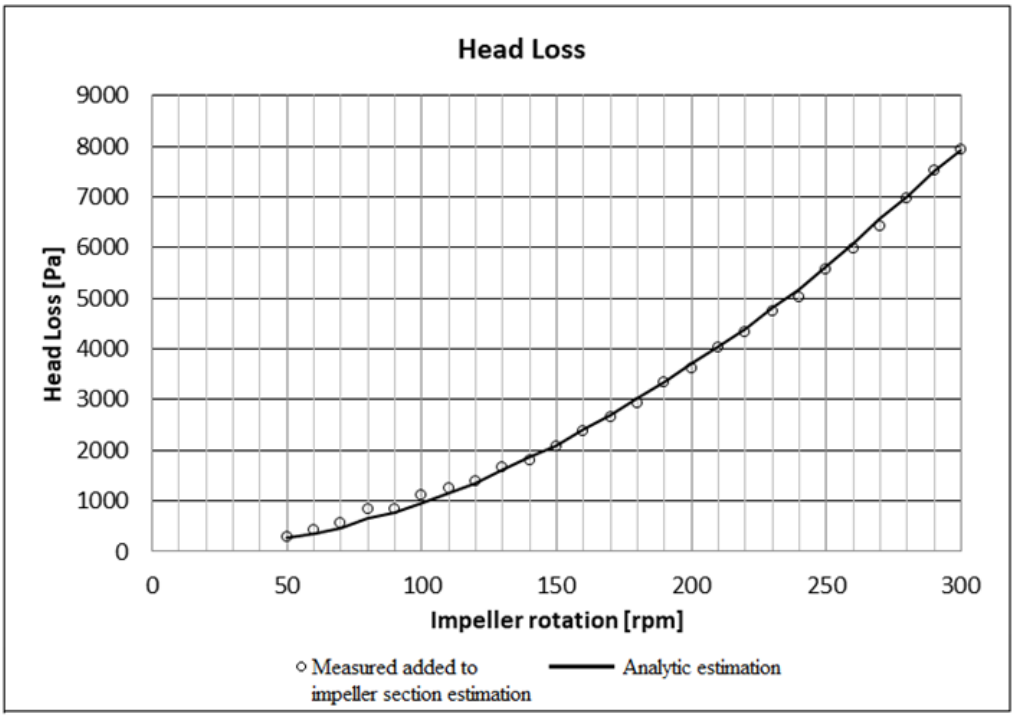

Figure 11. Comparison between total head loss (measured head loss added to impeller section estimation) and analytically estimated total head loss (according to Idelchik, 1986).

5.4 CFD computational results

The three meshes used for CFD simulations captured a very similar velocity profile. Figure 12 presents the velocity profile in the symmetry plane, where it is possible to notice a deceleration at the entrance of the contraction, acceleration at the entrance of the test section and the flow stabilization throughout the test section.

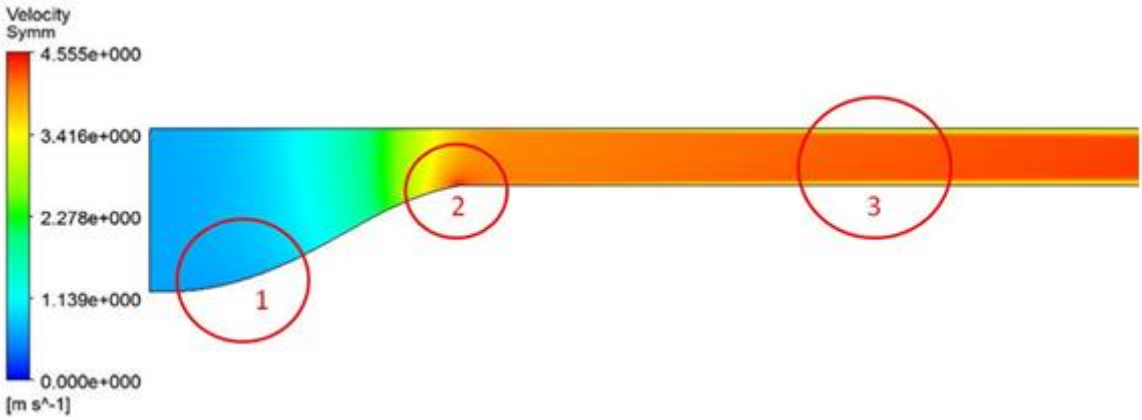

Figure 12.Velocity profile in the symmetry plane. 1) Deceleration at the entrance. 2) Acceleration at the entrance of the test section. 3) Flow stabilization.

Figure 13 presents the velocity profile in the middle of the test section, and Fig. 14 provides a comparison of the results for the three meshes in the same location where the experimental measurements where obtained.

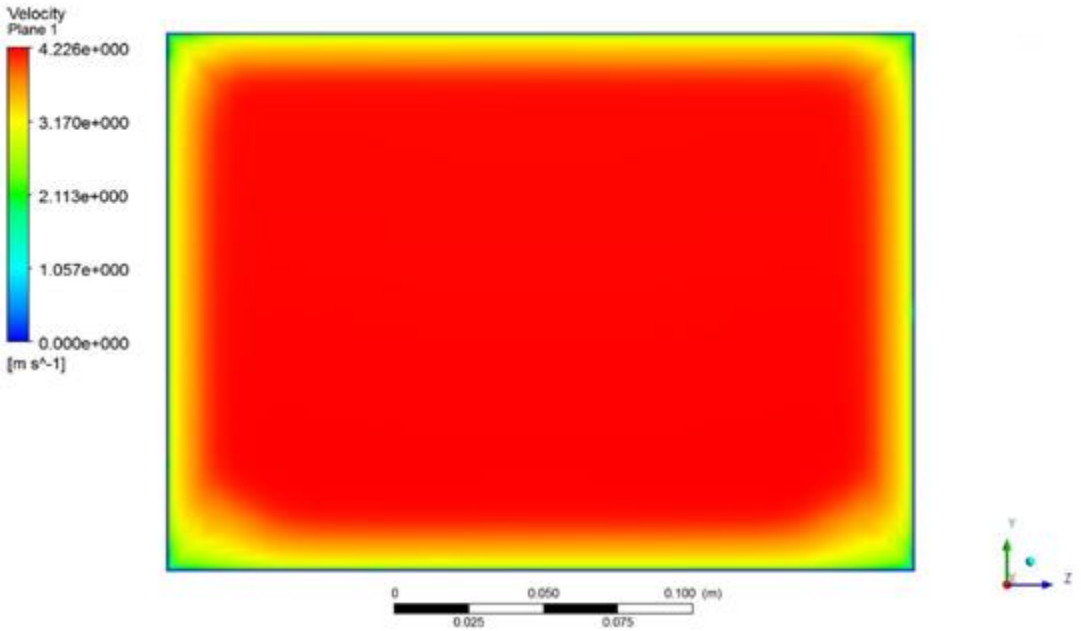

Figure 13.Velocity in the middle of the test section.

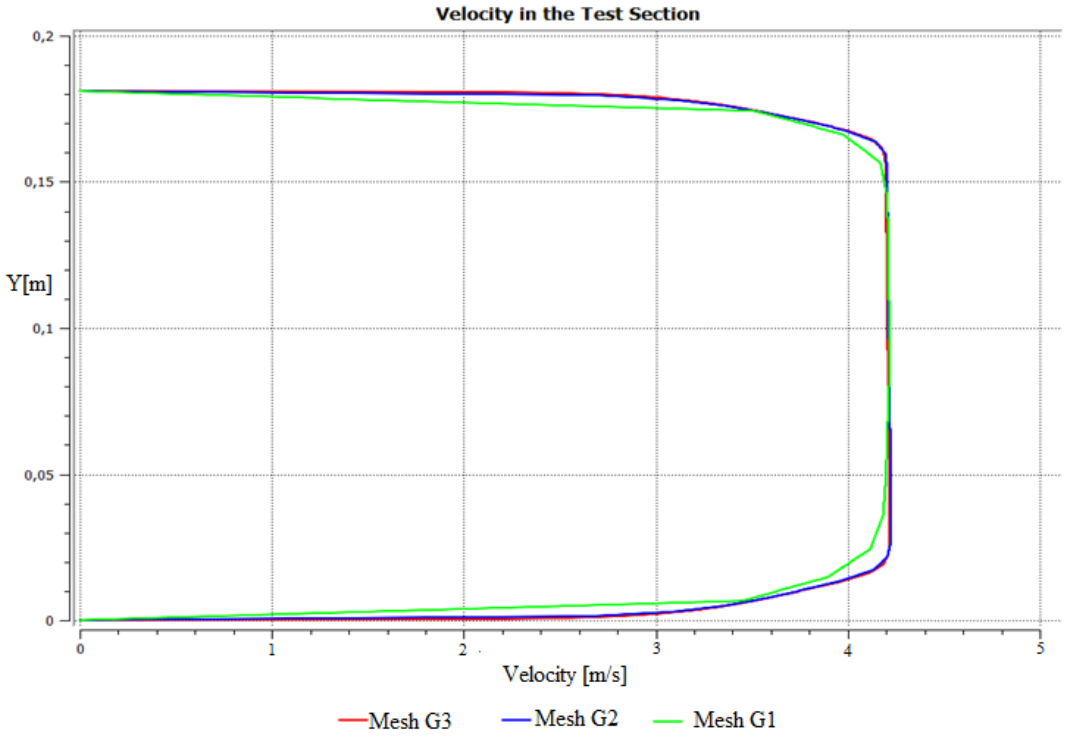

Figure 14. Comparison of velocity profile in the test section obtained with three different meshes, for a correspondent impeller rotation of 200 rpm.

Table 3 presents a comparison of the maximum values of velocity at the middle of the test section for the simulated meshes.

Table 3: Maximum velocity for the three meshes in the middle of the test section.

Mesh Id	Maximum Velocity [m/s]
G1	4,21542
G2	4,22505
G3	4,21936

5.5 Result discussion

The acoustic measurements identified the peak response of the second harmonic of the acoustic pressure in the impeller section. It was not possible to identify the first harmonic with the microphone, although this harmonic was captured by the hydrophone.

The measured results for the head loss agree well with the estimated head loss in all the impeller rotation range. The head loss estimation is key information for the impeller project, as it leads to the thrust needed for the water flow and shall be precise.

The measurement of the mean velocity in the test section and of the velocity profile provided data for comparison with the CFD simulation results.

The CFD results showed no significant difference in the more refined meshes G2 and G3, despite of a difference in the y+. The boundary layer obtained in the CFD simulation is around 20mm, which is smaller than the measured boundary layer, which is around 30mm. As a result, the mean velocity outside the boundary layer from the CFD simulation reached around 4.2m/s while the measured result reached around 4.4m/s, for the impeller rotation of 200 rpm.

It is possible to notice in the velocity profile that the boundary layer effects can be observed as the measurements get closer to the wall (160 mm and above from the center).The size of the boundary layer is smaller in the experimental results for the simulated velocity of 4.2 m/s.

6. CONCLUSION

LABHIDRO's Small Cavitation Tunnel (SCT) is a fundamental tool for the consolidation of the project methodology that is going to be used in the Large Cavitation Tunnel (TCGP). Its main purpose is to test the impeller concerning its hydrodynamic characteristics and its acoustic behavior. Among the tests performed in the SCT, the head loss, the acoustic measurements and the velocity profile measurements were described and compared with the analytical and simulation results. These tests allowed to verify that the analytical methods that are going to be used in the project of the Large Cavitation Tunnel (LCT) are reliable.

The acoustic measurements detect effects of blade pass frequency and is a tool for developing a low noise impeller. The project shall consider the use of skew in the impeller blades in order to reduce vibration and noise. Also, the number of blades shall be defined such that blade pass frequency noise is not amplified by the tunnel geometry when the impeller is operating in usual test speeds.

The mean velocity profile at the test section demonstrates a good behavior, with a small boundary layer. The velocity increases linearly with the impeller rotation. The CFD calculations for the test section should be improved in order to correctly estimate the boundary layer and the velocity profile in the test section.

Finally, the head loss measurements were obtained and verified with the analitic prediction. The estimation procedure is considered validated for the determination of the head loss of the LCT.

7. ACKNOWLEDGEMENTS

This work is supported by Diretoria de Desenvolvimento Nuclear da Marinha and by Centro Tecnológico da Marinha em São Paulo.

8. REFERENCES

Idelchik, I.E., 1986. *Handbook of Hydraulic Resistance*, Hemisphere Publishing Corporation, 2nd edition.

9. RESPONSIBILITY NOTICE

The authorsare the only responsible for the printed material included in this paper.